

# On the correlation of crystal defects and band gap properties of ZnO nanobelts

A. Asthana · K. Momeni · A. Prasad · Y.K. Yap · R.S. Yassar

Received: 24 April 2011 / Accepted: 22 July 2011 / Published online: 3 September 2011  
© Springer-Verlag 2011

**Abstract** We report here investigations of crystal and electronic structure of as-synthesized and annealed ZnO nanobelts by an in-situ high-resolution transmission electron microscope equipped with a scanning tunneling microscopy probe. The in-situ band gap measurements of individual ZnO nanobelts were carried out in scanning tunneling spectroscopy mode using the differential conductance  $dI/dV-V$  data. The band gap value of the as-synthesized ZnO nanobelts was calculated to be  $\sim 2.98$  eV, while this property for the annealed nanobelts ( $\sim 3.21$  eV) was close to the band gap value for bulk ZnO materials ( $\sim 3.37$  eV). The difference in the band gap value of the as-synthesized ZnO nanobelts and annealed ones was attributed to the planar defects (e.g. stacking faults and twins). These defects can alter the electronic structure by producing localized resonant states that result in band gap reduction.

One-dimensional (1D) ZnO nanostructures including nanowires and nanobelts are of great interest for field emission applications particularly for flat panel displays, as they can be synthesized in well-aligned densely packed arrays. With

a large exciton binding energy, thermal stability, oxidation resistance and favorable aspect ratio, ZnO nanowires and nanobelts are considered to be an effective field emission source [1–3]. The field emission properties of the nanostructured materials can be strongly influenced by the presence of localized resonant states [4]. Therefore, it is imperative to estimate the band gap of ZnO nanobelts used as field emission emitters. There has been number of studies to investigate the electronic band structure of ZnO in bulk and in thin-film form, using the techniques of photoluminescence spectroscopy and scanning tunneling microscopy [5–8]. To investigate the electronic properties, it is important that the measurements are carried out under a high-vacuum system, otherwise there are chances of oxide formation on the surface of the material, which will affect the electronic properties. Limited studies of the ZnO electronic band gap have been conducted in vacuum. One such study was carried out by Urbeita et al. [8] to investigate the electronic structure of ZnO single crystal in a combined scanning electron microscope (SEM)–scanning tunneling microscope (STM) system under a high vacuum of  $1 \times 10^{-6}$  Torr. In addition, one rarely can find nanoscale electrical measurements on single nanotubes or nanowires of ZnO. Most of the studies of the electronic structure of ZnO nanostructures have been carried out on arrays of nanowires/nanobelts by photoluminescence (PL) spectroscopy measurements taken at room temperature [9–13], but there are no reports on the electronic structure of individual ZnO nanowires/nanobelts.

In view of this, the present study is centered on the investigation of crystal and electronic structure correlation of individual nanobelts inside a high-resolution transmission electron microscope (TEM) (JEM 4000 FX, operated at 200 kV) using a special STM-TEM holder. The STM-TEM holder provides a unique combination of TEM and STM techniques, which are used simultaneously in one instrument for electrical and structural characterization. The

---

A. Asthana (✉) · K. Momeni · R.S. Yassar  
Department of Mechanical Engineering–Engineering Mechanics,  
Michigan Technological University, Houghton, MI 49931, USA  
e-mail: [aasthana@mtu.edu](mailto:aasthana@mtu.edu)

R.S. Yassar (✉)  
e-mail: [reza@mtu.edu](mailto:reza@mtu.edu)

A. Prasad · Y.K. Yap  
Physics Department, Michigan Technological University,  
Houghton, MI 49931, USA

Y.K. Yap  
e-mail: [ykyap@mtu.edu](mailto:ykyap@mtu.edu)

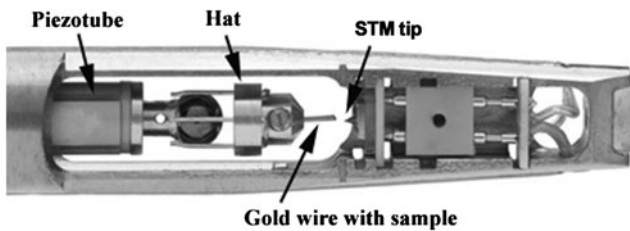


**Fig. 1** The image showing the experimental configuration for the STM-TEM holder

setup of the STM-TEM holder is shown in Fig. 1. The electrochemically etched gold wire with a ZnO nanobelt was attached to the piezo-driven movable part of the holder facing the fixed and sharp tungsten STM tip as its counter electrode, and oriented perpendicular to the electron beam in the TEM. In such an arrangement, atomic scale imaging and  $I$ - $V$  measurements can be carried out concurrently.

The ZnO nanobelts used in our study are grown in a double quartz tube configuration thermal chemical vapor deposition (CVD) system as reported previously but without the use of Au catalyst [14]. The growth was performed in a horizontal furnace consisting of a quartz tube vacuum chamber. A closed-end smaller quartz tube (60-cm long and 2 cm in diameter) containing the precursor materials and the substrates was inserted within the vacuum chamber. A mixture of ZnO (0.2 g) and graphite (0.1 g) powder in an alumina boat was used as the precursor materials. The boat is placed at the closed end of the smaller quartz tube. The temperature of the furnace was raised to 1100°C. The substrates are in a temperature zone of ~650 to 450°C. The temperature was held at 1100°C for 30 min and turned down to allow cooling to 600–700°C in ~1 h. The experiment is stopped by switching off the furnace and allowing the system to cool down to room temperature.

To have a good electrical circuit for tunneling measurement, the nanobelts should be firmly attached to the tip of the gold wire (250- $\mu$ m diameter) mounted on the piezotube shown in Fig. 1. To ensure this, the nanobelts were glued to the gold wire by conducting silver paste. In addition, the STM tip (made of tungsten, W) should be cleaned of any oxide layer to have a better electrical contact with the nanobelts. For this purpose, the side of the gold wire (without any sample) was moved into contact with the STM tip. The sharp W tip was readily melted on passing a large current through the tip, resulting in a clean W tip with slightly larger radius.

The STM was used in constant-current mode as well as in the scanning tunneling spectroscopy (STS) mode. The STM measurements were performed by measuring the tunneling current ( $I$ ) and dynamic conductance ( $dI/dV$ ) as a function of tip-sample voltage at a fixed tip-sample distance. The STS provides real-space imaging of electronic states by recording  $dI/dV$ - $V$  curves at fixed tip-sample separation [15, 16]. Spectroscopy measurements reported here are

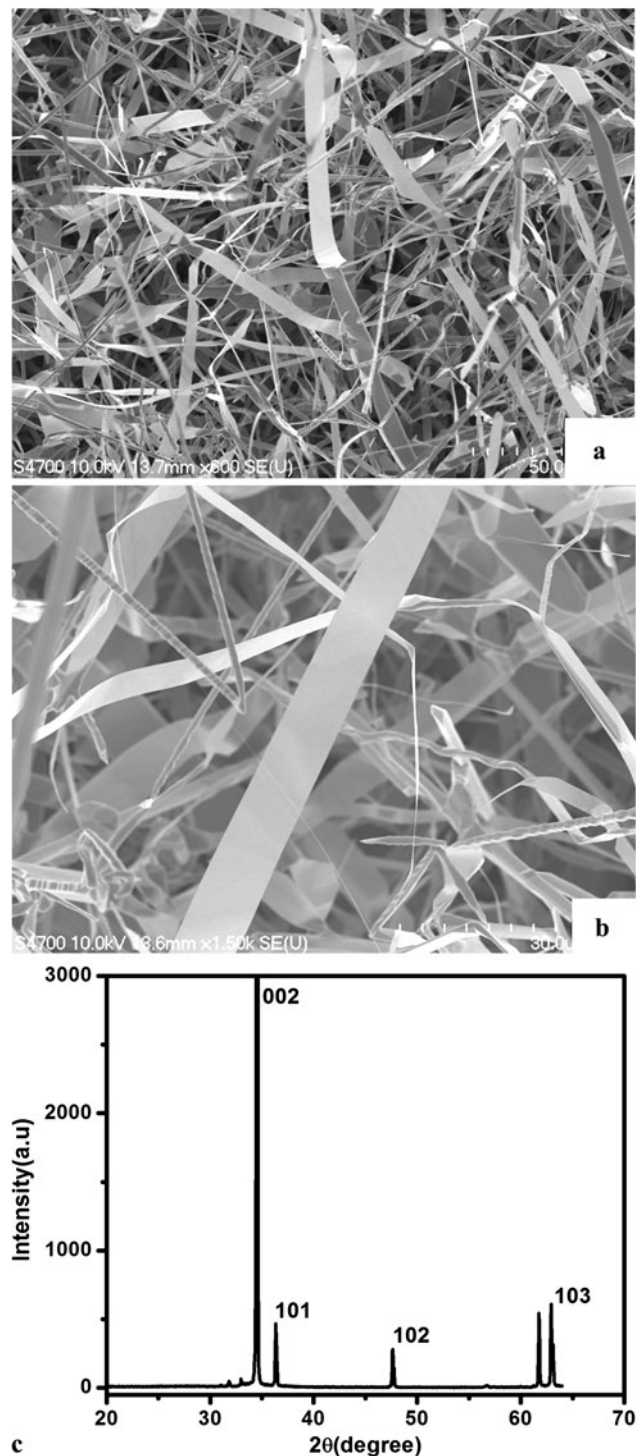
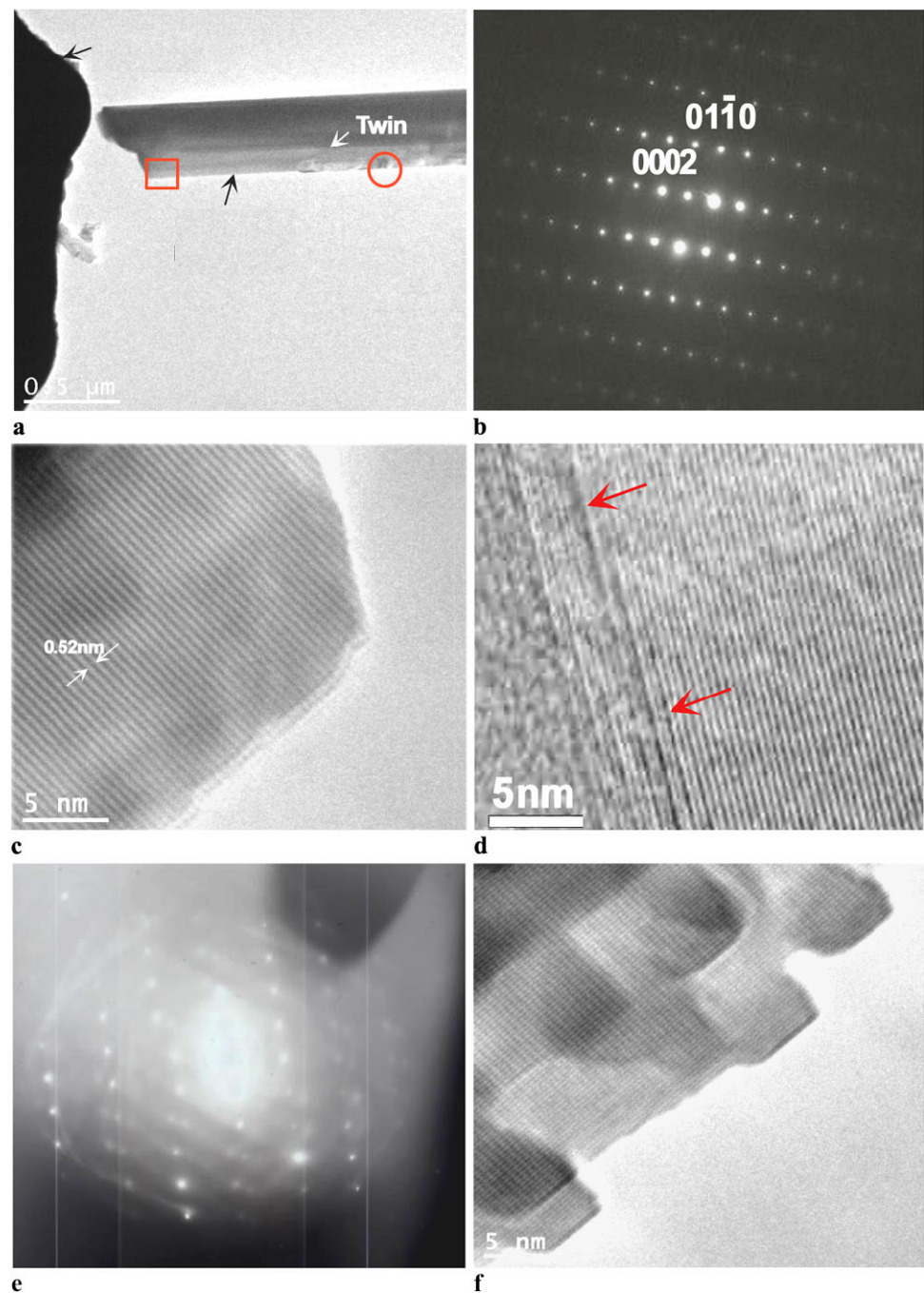


**Fig. 2** (a) The low-magnification SEM image of a ZnO nanobelt showing the overall morphology. (b) Zoomed-in image of the nanobelts showing two distinct widths along their length. (c) The XRD pattern of the as-synthesized ZnO nanobelts showing the crystallinity of the nanobelts

obtained by averaging five to 10 tunneling current ( $I$ ) versus bias voltage ( $V$ ) curves at specific locations on the ZnO nanobelts. The data are represented by using the ratio of differential to total conductance,  $(dI/dV)/(I/V)$ , that gives

**Fig. 3** (a) A low-magnification TEM image of a ZnO nanobelt; (b) the selected area electron diffraction (SAED) pattern of the nanobelt taken along the  $[01\bar{1}0]$  zone axis; (c) HRTEM image of the nanobelt taken from the selected area (marked by *rectangle*); (d) HRTEM image of a nanobelt showing the planar defects; (e) the diffraction pattern taken from the twin-boundary region; (f) HRTEM image of the nanobelt showing the steps at the edge



a direct measure of the surface density of states [17–19]. The curves represent the average of data recorded in small regions, typically a square of 10 pixels on each side. The spectroscopic measurements were found to be reproducible.

The nanobelts grown on Si (100) single-crystal substrates were directly observed by a field emission scanning electron microscope (SEM, Hitachi S-4700). Figure 2a and b show typical SEM images of the grown nanobelts. The top view (Fig. 2b) clearly reveals that the film is composed of belt-like nanostructures with typical lengths in the range of several hundreds of nanometers to several micrometers and widths

ranging from 1 to 5  $\mu\text{m}$ . X-ray diffraction (XRD) measurements were carried out on a RINT 2500 X-ray diffractometer using  $\text{CuK}\alpha$  radiation. Figure 2c shows the XRD pattern of the as-synthesized ZnO nanobelt confirming its purity and high crystallinity. All the peaks in the pattern can be indexed to the wurtzite ZnO structural phase with  $a = 0.32$  nm and  $c = 0.52$  nm, with no apparent impurity phase. It is worth noting that the peak intensity of the (002) plane is about 10 times as high as that of (101) planes. This is consistent with the alignment growth of the nanobelts on Si substrates and

their preferential growth along the [0001] direction, as also confirmed in our TEM observations.

The detailed structure of ZnO nanobelts was characterized just before the in-situ STM-TEM measurements. Figure 3a presents a low-magnification TEM image of a ZnO nanobelt. The length and width of the nanobelt were measured to be  $\sim 2 \mu\text{m}$  and 400 nm, respectively (Fig. 3a). The selected area electron diffraction (SAED) pattern (Fig. 3b) confirms the single-crystalline nature of the nanobelt and is indexed to be the [01 $\bar{1}$ 0] zone axis of wurtzite ZnO. The growth direction of [0001] can be easily established from the SAED pattern in Fig. 3b. Figure 3c shows a high-resolution TEM (HRTEM) image of the nanobelt taken from a selected area (marked by the red rectangle) and reveals the crystalline lattice of the nanobelt. The distance between lattice planes is approximately 0.52 nm. However, some regions of the nanobelt show a change in the stacking sequence over a few atomic spacings and depict the presence of stacking faults, a planar defect (marked by the arrow in the HRTEM image, Fig. 3d). The nanobelt also shows another type of planar defect, the twin boundary (marked by the white arrow in Fig. 3a) that is confirmed by the diffraction pattern taken from the twin-boundary region as shown in Fig. 3e. The presence of such defects in ZnO nanobelts has also been reported by Wang and Ding [20, 21]. Also, some of the nanobelts show the formation of steps at the edge (Fig. 3f). As evident from the HRTEM image, the steps are entirely single-crystalline and defect-free in nature, with some roughness at the edge of the nanobelts.

The elemental mapping and the compositions were measured by energy dispersive X-ray spectrometry (EDS) equipped in the TEM. The elemental mapping was conducted in scanning transmission mode of the TEM. The EDS analysis and the elemental mapping images (Fig. 4) showed the presence of Zn in the ZnO nanobelts. No other elements were detected. This confirms that high-purity ZnO nanobelts have grown on Si crystal substrates. Oxygen mapping could not be observed due to limitation of the EDS measurements.

The vacuum barrier between the STM tip and the nanobelt forms a convenient junction for STS, as it allows tunnel current at large bias voltages. In STS, scanning and feedback controls were switched off, and current,  $I$ , was recorded as a function of bias voltage,  $V$ , applied to the nanobelt. The normalized differential conductance  $(dI/dV)/(I/V)$  can then be considered to be proportional to the density of states (DOS) of the examined nanobelt. Before and after taking STS measurements on the nanobelt, reference measurements were performed on the gold wire. Only when the curves on gold wire were approximately linear without kinks or steps were the  $I$ - $V$  data on the nanobelt recorded. The STS curves taken at different positions (typically over  $\sim 40$  nm) showed consistent features. Figure 5a and b and c and d show the corresponding  $I$ - $V$  curves and

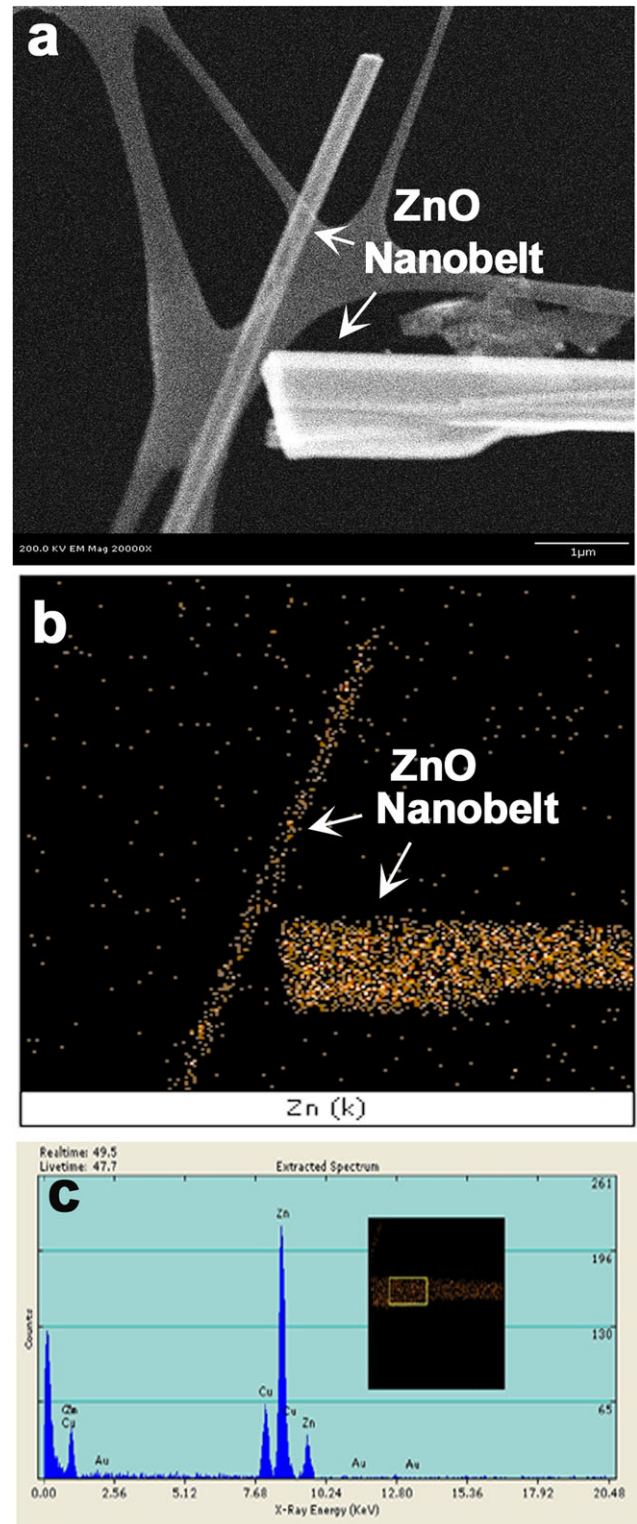
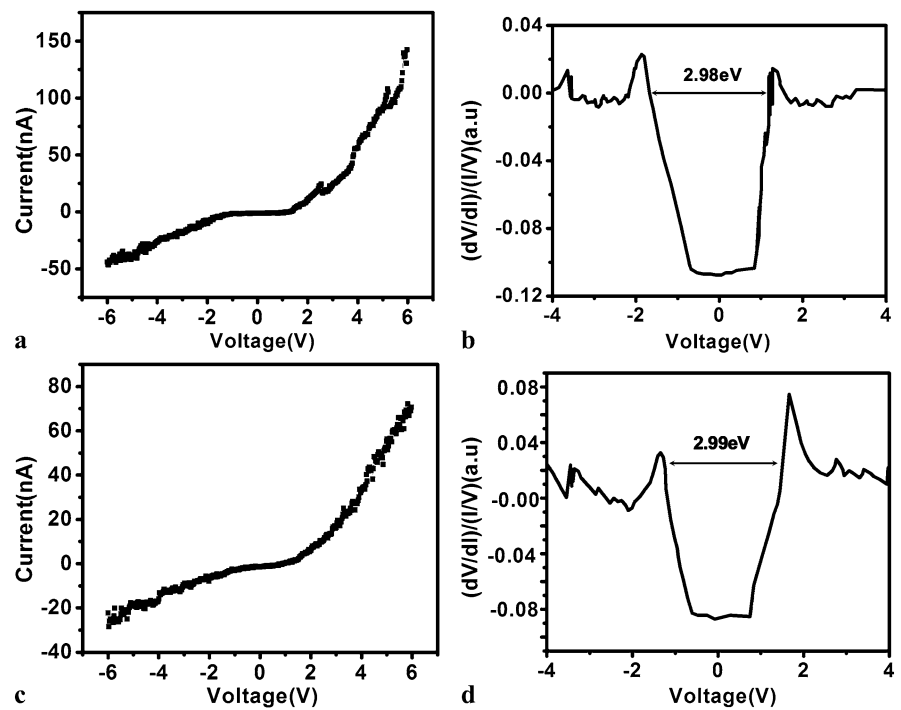


**Fig. 4** (a) The scanning transmission electron microscopy (STEM) image of a ZnO nanobelt; (b) the STEM image showing the mapping of Zn elements in the ZnO nanobelt; (c) the EDS data confirms the presence of Zn in the ZnO nanobelt

**Fig. 5** (a, b) and (c, d) show the corresponding  $I-V$  curve and  $dI/dV-V/(I/V)$  obtained by STS on two different as-synthesized nanobelts



normalized conductance,  $(dI/dV)/(I/V)-V$ , on two different as-synthesized nanobelts. The corresponding  $I-V$  curve shows a low conductance at low bias, followed by several kinks at larger bias voltages. The average value of the band gap obtained from the normalized differential conductance  $(dI/dV)/(I/V)-V$  for the as-synthesized nanobelts (averaged over eight nanobelts) is  $\sim 2.98 \pm 0.2$  eV. The band gap value estimated for the as-synthesized ZnO nanobelt ( $\sim 2.98$  eV) is about 11.57% less than the standard value obtained for the ZnO materials, i.e. 3.37 eV [22]. This difference can be attributed to the planar defects like stacking faults and twin boundaries observed in the ZnO nanobelts confirmed by high-resolution images (Fig. 3). These kinds of defects are expected to alter the electronic structure by producing localized resonant states [9, 23–25]. Beside these, the ZnO materials are also known to possess intrinsic defects, such as oxygen vacancies, zinc vacancies and Zn and O interstitials, etc. [26–28], which will also affect the electronic structure of ZnO. For comparison, the tunneling data for the annealed ZnO nanobelt was also measured as shown in Fig. 6a–c. Figure 6a shows the bright-field image of the annealed ZnO nanobelt. As is evident from Fig. 6a, most of the regions of the annealed nanobelt show no image contrast, indicating a defect-free region. The annealed ZnO nanobelts show the estimated value of the band gap to be  $\sim 3.21 \pm 0.15$  eV. The annealed ZnO nanobelt shows  $\sim 7.16\%$  higher value of band gap as compared to the as-synthesized sample, which indicates that annealing of the ZnO nanobelt at  $600^\circ\text{C}$  for 15 min in hydrogen atmosphere decreases the intrinsic defects present in the as-synthesized sample [29].

From the normalized differential conductance data,  $(dI/dV)/(I/V)-V$ , it is observed that the band gap is symmetrical about the zero bias position, which indicates that there is no doping of any type of carrier (i.e. p or n type) in the ZnO nanobelt during the measurement. In a report [30] on the band gap measurements of carbon nanotubes by STM, the asymmetry of the  $(dI/dV)/(I/V)-V$  data around zero bias voltage was related to the doping of carbon nanotubes by charge transfer from the Au (111) substrate on which the nanotubes were grown. In the present investigation, the ZnO nanobelts were tested in free-standing condition, which is consistent with the absence of any asymmetry of the band gap around the zero bias voltage. The derivative spectra indeed show a number of peaks (Figs. 5b, 5d and 6c). The peaks differ in height depending on the region of the STM tip chosen and hence its configuration. In semiconductors,  $(dI/dV)/(I/V)$  has been argued to give a better representation of the DOS than the direct derivative  $dI/dV$ , partly because the normalization accounts for the voltage dependence of the tunnel barrier at high bias [31–34].

In conclusion, the electronic band gap measurement of an individual ZnO nanobelt was carried out in situ in a combined STM-TEM system. To the authors' knowledge, this is the first in-situ TEM study of the band gap properties of individual ZnO nanobelts. The normalized differential electrical conductance,  $(dI/dV)/(I/V)$ , of the nanobelt measurement in STS mode provides a direct measurement of the band gap. The average value of the band gap of individual as-synthesized ZnO nanobelts has been estimated to be  $\sim 2.98 \pm 0.2$  eV, which is about 11.57% smaller than

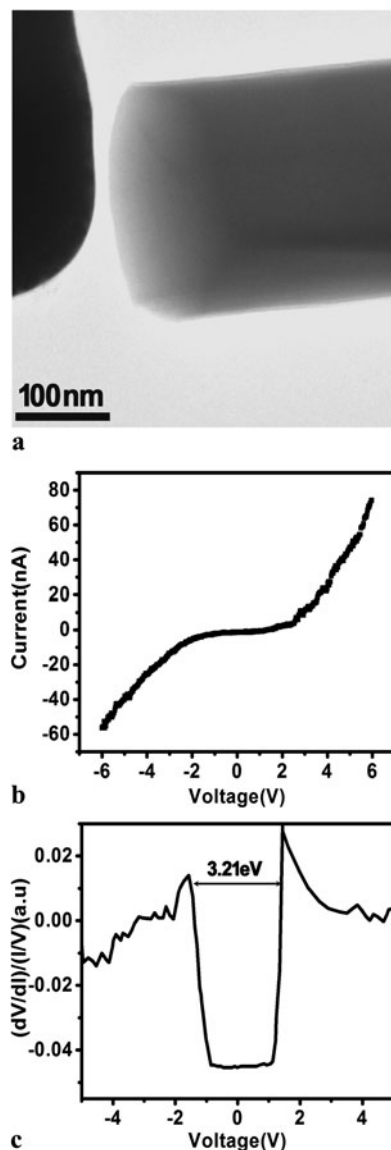


**Fig. 6** (a) The bright-field image of an individual annealed nanobelt attached firmly with the gold tip and facing the counter electrode, the STM tip. (b and c) The corresponding  $I$ - $V$  curve and  $dI/dV$ - $V/(I/V)$  obtained by STS on the nanobelt

the standard value of  $\sim 3.37$  eV obtained from the bulk ZnO materials. The annealed ZnO nanobelt shows a higher value of the band gap ( $\sim 3.21 \pm 0.15$  eV) as compared to the as-synthesized sample. This indicates that annealing decreases the intrinsic defects present in the as-synthesized sample. The smaller band gap value in the as-synthesized ZnO nanobelt was attributed to planar defects, like stacking faults, twin boundaries observed in the ZnO nanobelts by high-resolution images and intrinsic defects like oxygen vacancies, zinc vacancies and Zn and O interstitials found in ZnO materials.

**Acknowledgement** The authors would like to acknowledge the funding support through the NSF-DMR grant no. 0820884 and the NSF-CMMI grant no. 0926819.

## References

1. W.A. de Heer, A. Chatelain, D. Ugarte, *Science* **270**, 1197 (1995)
2. S. Fan, M.G. Chaplin, N.R. Franklin, T.W. Tomblor, A.M. Cassell, H. Dai, *Science* **283**, 512 (1999)
3. L. Nilsson, O. Groening, C. Emmenegger, O. Kuettel, E. Schaller, L. Schlapbach, *Appl. Phys. Lett.* **76**, 2071 (2000)
4. W.A. de Heer, J.-M. Bonard, K. Fauth, A. Chatelain, L. Forro, D. Ugarte, *Adv. Mater.* **9**, 87 (1997)
5. A.P. Roth, J.B. Webb, D.F. Williams, *Phys. Rev. B* **25**, 7836 (1982)
6. Y.F. Lu, H.Q. Ni, Z.H. Mai, Z.M. Ren, *J. Appl. Phys.* **88**, 498 (2000)
7. V. Srikant, D.R. Clarke, *J. Appl. Phys.* **83**, 5447 (1998)
8. A. Urbeita, P. Fernandez, J. Piqueras, T. Sekiguchi, *Semicond. Sci. Technol.* **16**, 589 (2001)
9. Y.B. Li, Y. Bando, T. Sato, K. Kurashima, *Appl. Phys. Lett.* **81**, 144 (2002)
10. B. Lin, Z. Fu, Y. Jia, *Appl. Phys. Lett.* **79**, 943 (2001)
11. H. Mao, K. Yu, J. Wang, J. Yu, Z. Zhu, *Opt. Express* **17**, 118861 (2009)
12. S. Ruhle, L.K. van Vugt, H.Y. Li, N.A. Keizer, L. Kuipers, D. Vanmaekelbergh, *Nano Lett.* **8**, 119 (2008)
13. L.X. Sun, Z.H. Chen, Q. Ren, K. Yu, L. Bai, W. Zhu, H. Xiong, Z.Q. Zhu, X. Shen, *Phys. Rev. Lett.* **100**, 156403 (2008)
14. S.L. Menshah, V.K. Kayastha, Y.K. Yap, *J. Phys. Chem. C* **111**, 16092 (2007)
15. R.M. Feenstra, *Surf. Sci.* **965**, 299 (1994)
16. J.A. Stroscio, R.M. Feenstra, A.P. Fein, *Phys. Rev. Lett.* **57**, 2579 (1986)
17. N.D. Lang, *Phys. Rev. B* **34**, 5497 (1986)
18. R.M. Feenstra, J.A. Stroscio, A.P. Fein, *Surf. Sci.* **181**, 295 (1987)
19. R.J. Hamers, R.M. Tramp, J.E. Demuth, *Phys. Rev. Lett.* **56**, 1972 (1986)
20. Y. Ding, Z.L. Wang, *Micron* **40**, 335 (2009)
21. Z.L. Wang, *Mater. Sci. Eng., R Rep.* **64**, 33 (2009)
22. C. Kligshirn, *Phys. Status Solidi B* **71**, 547 (1975)
23. H.Y. Peng, M.D. McCluskey, Y.M. Gupta, M.A. Kneissl, N.M. Johnson, *Phys. Rev. B* **71**, 1152071 (2005)
24. K. Nishidate, M. Hasegawa, *Phys. Rev. B* **78**, 195403 (2008)
25. S.D. Mahanti, K. Hoang, S. Ahmad, *Physica B* **401**, 291 (2007)
26. E.G. Bylander, *J. Appl. Phys.* **49**, 1188 (1978)
27. K. Vanheusden, C.H. Seager, W.L. Warren, D.R. Tallant, J.A. Voigt, *Appl. Phys. Lett.* **68**, 403 (1996)
28. M. Liu, A.H. Kitai, P. Mascher, *J. Lumin.* **54**, 35 (1992)
29. A. Prasad, A. Pandey, Y.K. Yap, *Bull. Am. Phys. Soc.* **55**, 292 (2010)
30. J.W.G. Wildoer, L.C. Venema, A.G. Rinzler, R.E. Smalley, C. Dekker, *Nature* **391**, 59 (1998)
31. J.A. Stroscio, R.M. Feenstra, A.P. Fein, *Phys. Rev. Lett.* **57**, 2579 (1986)
32. R.M. Feenstra, J.A. Stroscio, A.P. Fein, *Surf. Sci.* **181**, 295 (1987)
33. N.D. Lang, *Phys. Rev. B* **34**, R5947 (1986)
34. R.J. Hamers, in *Scanning Tunneling Microscopy and Spectroscopy*, ed. by D.A. Bonnelli (VCH, New York, 1993), pp. 51–103